

Article

Microstructural Optimization of Sn-58Bi Low-Temperature Solder Fabricated by Intense Pulsed Light (IPL) Irradiation

Hyeri Go ¹, Taejoon Noh ², Seung-Boo Jung ² and Yoonchul Sohn ^{1,*} 

¹ Department of Welding & Joining Science Engineering, Chosun University, 309 Pilmoon-daero, Dong-gu, Gwangju 61452, Republic of Korea; heili1235@chosun.ac.kr

² School of Advanced Materials Science and Engineering, Sungkyunkwan University, 2066 Seobu-ro, Jangan-gu, Suwon 16419, Republic of Korea; hokujoon@skku.edu (T.N.); sbjung@skku.edu (S.-B.J.)

* Correspondence: yoonchul.son@chosun.ac.kr

Abstract: In this study, intense pulsed light (IPL) soldering was employed on Sn-58Bi solder pastes with two distinct particle sizes (T3: 25–45 μm and T9: 1–8 μm) to investigate the correlation between the solder microstructure and mechanical properties as a function of IPL irradiation times. During IPL soldering, a gradual transition from an immature to a refined to a coarsened microstructure was observed in the solder, impacting its mechanical strength (hardness), which initially exhibited a slight increase followed by a subsequent decrease. It is noted that hardness measurements taken during the immature stage may exhibit slight deviations from the Hall–Petch relationship. Experimental findings revealed that as the number of IPL irradiation sessions increased, solder particles progressively coalesced, forming a unified mass after 30 sessions. Subsequently, after 30–40 IPL sessions, notable voids were observed within the T3 solder, while fewer voids were detected at the T9-ENIG interface. Following IPL soldering, a thin layered structure of Ni_3Sn_4 intermetallic compound (IMC) was observed at the Sn-58Bi/ENIG interface. In contrast, reflow soldering resulted in the abundant formation of rod-shaped Ni_3Sn_4 IMCs not only at the reaction interface but also within the solder bulk, accompanied by the notable presence of a P-rich layer beneath the IMC.



Citation: Go, H.; Noh, T.; Jung, S.-B.; Sohn, Y. Microstructural Optimization of Sn-58Bi Low-Temperature Solder Fabricated by Intense Pulsed Light (IPL) Irradiation. *Crystals* **2024**, *14*, 465. <https://doi.org/10.3390/cryst14050465>

Academic Editors: Reza Beygi, Mahmoud Moradi, Ali Khalfallah and Marek Sroka

Received: 31 March 2024

Revised: 23 April 2024

Accepted: 15 May 2024

Published: 16 May 2024



Copyright: © 2024 by the authors. Licensee MDPI, Basel, Switzerland. This article is an open access article distributed under the terms and conditions of the Creative Commons Attribution (CC BY) license (<https://creativecommons.org/licenses/by/4.0/>).

Keywords: intense pulsed light; Sn-58Bi; solder; Hall–Petch relationship; microstructure

1. Introduction

Modern electronic packaging technology, which facilitates the interconnection of semiconductor chips and packages through solder bonding, stands as a pivotal component in ensuring device reliability [1–5]. While conventional reflow soldering techniques utilizing convection ovens have been extensively employed, there is a persistent drive to address substrate warpage stemming from disparate coefficients of thermal expansion among electronic package materials, alongside endeavors to curtail soldering expenses [6,7]. This impetus has fueled the continual evolution of technologies such as laser-assisted bonding (LAB) and intensive pulsed light (IPL) soldering.

LAB technology, exploiting a laser wavelength that exhibits heightened absorption characteristics in Si chips relative to polymer materials, offers the notable advantage of mitigating substrate heating and minimizing warpage [8–10]. Through decades of dedicated research, a repertoire of materials and methodologies applicable to LAB, including flux-free underfills, has been cultivated. Nonetheless, LAB equipment is encumbered by the requisite inclusion of a homogenizer to transform the laser point source into a planar source, and achieving large-area irradiation poses a formidable challenge. Conversely, IPL technology has traditionally found utility in aggregating and sintering minute nanoparticles via diffusion-mediated reactions. Recently, there has been a burgeoning interest in repurposing this technology for soldering processes. These advancements underscore the relentless pursuit within the electronic packaging industry of ways to bolster the reliability of soldering operations, address substrate warpage concerns, and optimize cost efficiency.

Only a limited number of documented instances involve the application of IPL soldering to Sn-based solder formulations within operational electronic packages [11–16]. Jung et al. [11] presented findings detailing the IPL soldering of Sn-58Bi, illustrating a mere 2.5% duration requirement relative to conventional reflow techniques, alongside a 40% enhancement in mechanical strength. Ha et al. [12] conducted an evaluation of the reliability impact on Sn-3.0Ag-0.5Cu ball grid array (BGA) packages with Electroless Nickel Electroless Palladium Immersion Gold (ENEPIG) surface treatment, employing the IPL soldering methodology. Experimental observations under optimized IPL parameters revealed an approximate 6.7-fold increase in the number of failure cycles compared to reflow soldering. Furthermore, Min et al. [13] provided comprehensive experimental results contrasting IPL soldering against conventional reflow soldering. Their analysis indicated significantly lower power consumption during the IPL radiation soldering process (17.95 kWh) compared to the traditional convection reflow process (29.50 kWh). Moreover, IPL-soldered joints exhibited a substantial improvement in drop impact reliability (with a recorded number of drops to failure of 277) compared to reflow-soldered joints (with a recorded number of drops to failure of 103). These findings underscore the considerable potential of IPL soldering in reducing process duration, controlling intermetallic compound (IMC) thickness to enhance drop impact reliability, and optimizing power consumption.

In addition to the aforementioned advantages, IPL soldering exhibits distinctive attributes. For instance, in reflow soldering, post-process grain growth in solders is prominently observed. Conversely, the IPL process affords facile manipulation of the degree to which metal particles constituting the solder paste are liquefied, through adjustments in process parameters such as frequency, pulse width, and intensity. This inherent flexibility facilitates the generation of varied microstructural configurations, spanning from refined microstructures with diminutive grain sizes to those characterized by larger grain dimensions. In this study, meticulous scrutiny of the microstructural evolution of Sn-58Bi solder paste was undertaken, spanning from its nascent stages to later stages of reaction. The investigation encompassed an analysis of the correlation between grain size and resultant mechanical properties. It is posited that such investigations furnish valuable insights pertinent to future applications of IPL in soldering processes.

2. Materials and Methods

Two distinct sizes of Sn-58Bi solder paste were procured from BBEIN: type 3 (BBI-LESP04, 25–45 μm) and type 9 (BBI-NCLFSP048, 1–8 μm). A printed circuit board (PCB) featuring Electro-less Nickel Immersion Gold (ENIG)-treated 400 μm metal pads was fabricated for substrate application, possessing dimensions of 77 \times 132 mm^2 with a 6 \times 12 array for ball alignment. Solder paste deposition onto the PCB was facilitated using a metal mask with a thickness of 0.2 mm. For IPL soldering, the charge voltage and peak current were maintained at 1500 V and 2000 A, respectively. The IPL irradiation area spanned 20 \times 30 cm^2 . Process variables for IPL, including frequency and pulse width, were set at 3 Hz and 2.0 ms, respectively, with IPL irradiation sessions ranging from 10 to 70 during soldering operations. Figure 1 provides a graphical representation of the IPL process variable configurations for enhanced comprehension. Furthermore, the experimental parameters utilized in this investigation are summarized in Table 1. Depending on the experimental conditions, the applied energy increased proportionally with IPL irradiation sessions, ranging from 100 to 700 J/cm^2 , while maintaining a consistent power consumption of 18 kWh.

For comparative analysis, a reflow-soldered joint was fabricated utilizing a reflow machine (model: BT301N) manufactured by Autotronik-SMT GmbH, Amberg, Germany. The peak temperature during reflow was set at 180 $^{\circ}\text{C}$, and the specific reflow profile employed in the experimental setup is delineated in Figure 2. Microstructural and compositional characterization of the solder joints was conducted utilizing field emission scanning electron microscopy (FE-SEM, model: JEOL JSM-7900) coupled with energy dispersive spectroscopy (EDS, model: JEOL JXA-8500F). The thickness of the IMC in the SEM micrographs was

quantified by employing image analysis software, whereby the thickness of the IMC layer was defined as the total area occupied by the phase divided by its length. Average thickness values were derived from measurements acquired from six distinct regions within each reaction specimen. Electron Backscattered Diffraction (EBSD) analysis was performed utilizing FE-SEM (model: HITACHI S-5000) equipped with EDAX Velocity super. The hardness of the solder joints post-IPL irradiation was assessed utilizing MMT-X7A equipment from MATSUZAWA. The hardness assessment involved the averaging of measurements taken at six distinct locations for each solder, with a measurement interval of 100 μm , using a load of 5 gf and a dwell time of 10 s.

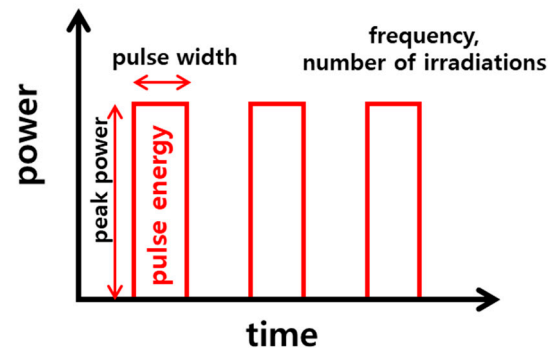


Figure 1. Process variables for IPL soldering.

Table 1. IPL soldering conditions and sample identification.

| Sample ID | Frequency | Pulse Width | Number of IPL Irradiation | Total Energy | Power Consumption | Time |
|-----------|-----------|-------------|---------------------------|----------------------|-------------------|-------|
| | (Hz) | (ms) | (n) | (J/cm ²) | (kWh) | (sec) |
| IPL 10 | 3 | 2 | 10 | 100 | 18 | 3.3 |
| IPL 20 | 3 | 2 | 20 | 200 | 18 | 6.6 |
| IPL 30 | 3 | 2 | 30 | 300 | 18 | 9.9 |
| IPL 40 | 3 | 2 | 40 | 400 | 18 | 13.2 |
| IPL 50 | 3 | 2 | 50 | 500 | 18 | 16.5 |
| IPL 60 | 3 | 2 | 60 | 600 | 18 | 19.8 |
| IPL 70 | 3 | 2 | 70 | 700 | 18 | 23.1 |
| reflow | | | | | | 600 |

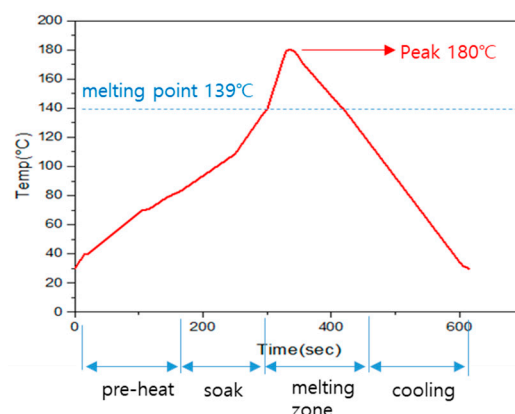


Figure 2. Reflow profile for Sn-58Bi soldering.

3. Results and Discussion

3.1. Microstructural Evolution during IPL Soldering

When IPL soldering was conducted under the prescribed conditions of a 3 Hz frequency and a 2 ms pulse width, the evolution of macrostructural features in Sn-58Bi solder

paste was observed as a function of the number of IPL irradiation sessions, as illustrated in Figure 3. Following 10 IPL irradiation sessions, it is evident that a substantial portion of both type 3 (T3) and type 9 (T9) solder paste particles remained unmelted, retaining their initial particle size distribution. Notably, in the case of T9, partial melting and recombination of particles can be observed predominantly in the upper region, resulting in an enlargement of particle dimensions from the initial 1–8 μm range to several tens of micrometers.

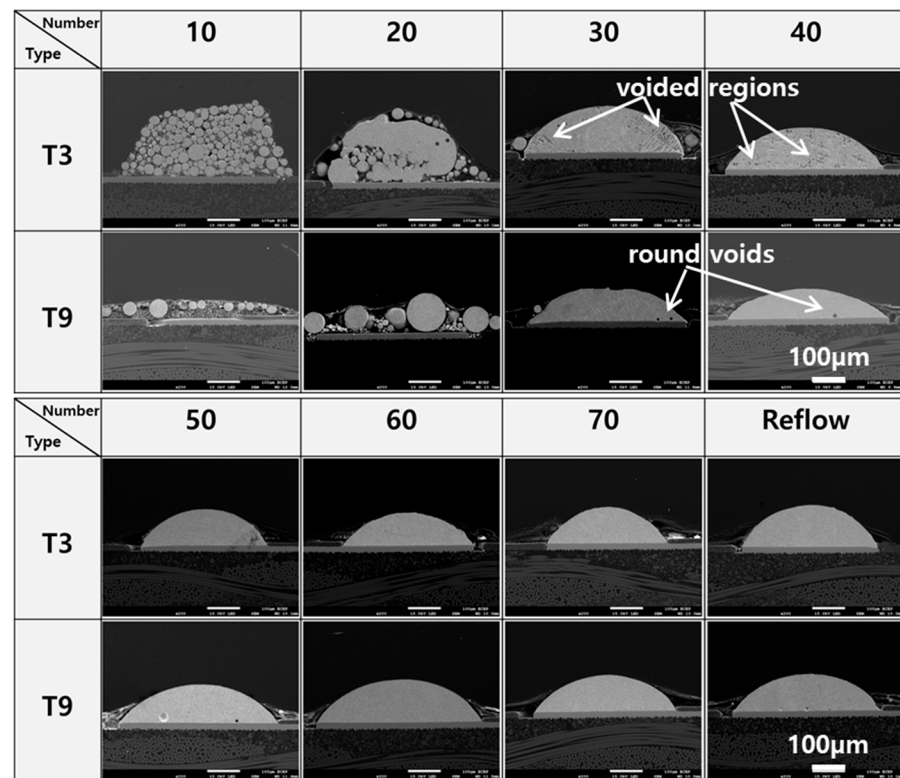


Figure 3. Macroscopic morphological changes in Sn-58Bi solder pastes with increasing sessions of IPL irradiation (3 Hz, 2 ms).

After 20 IPL irradiation sessions, notable particle bonding occurred, particularly evident in the T3 solder paste despite its larger initial particle size. Significant solder lump formation, primarily concentrated in the upper portion, can be observed, with partial lump formation occurring in regions interfacing with the ENIG substrate. Notably, remnants of smaller particles persist in the mid-section. Conversely, in T9, the agglomeration phenomenon initiated in the uppermost region propagates downward, albeit with limited advancement observable at the lower extremity.

Following 30 IPL irradiation sessions, complete fusion of solder particles from both T3 and T9 culminated in the formation of a singular, substantial solder bump. Subsequent to 30–40 IPL irradiation sessions, a considerable prevalence of voids can be observed within the T3 solder bump, whereas T9 exhibits only sparse, round voids primarily localized at the lower extremity of the solder bump. The occurrence of voids during IPL soldering can be attributed to the size and aggregation process of the initial solder particles in the solder paste, as well as the wetting characteristics on ENIG, the substrate surface treatment. In the T3 sample, substantial aggregates form as a unified entity, with voids emerging in between, whereas in the T9 sample, initial formation comprises small and medium-sized aggregates that subsequently coalesce into a single large aggregate. Notably, for the T9 sample, the initial solder particle size is smaller, and there is improved spreading on ENIG, resulting in a minimal occurrence of voids. Beyond 50 IPL irradiation sessions, both T3 and

T9 configurations manifest a densified microstructure with minimal void formation, with discernible convergence in structural characteristics.

Under the conditions of a 3 Hz frequency and a 2.0 ms pulse width, the alterations in the microstructural characteristics of Sn-58Bi solder paste as a function of the number of IPL irradiation sessions were as depicted in Figure 4. Initial inspection of the Sn-58Bi solder particles after 10–20 IPL sessions revealed a notably finer microstructure in type 9 (T9) compared to type 3 (T3). Notably, the bright, protruding regions within the solder particles corresponded to Bi, while the darker, recessed regions represented Sn, forming an alternately arranged lamellar structure. The lamellar width was in the order of several micrometers in T3, whereas it diminished to submicron dimensions in T9.

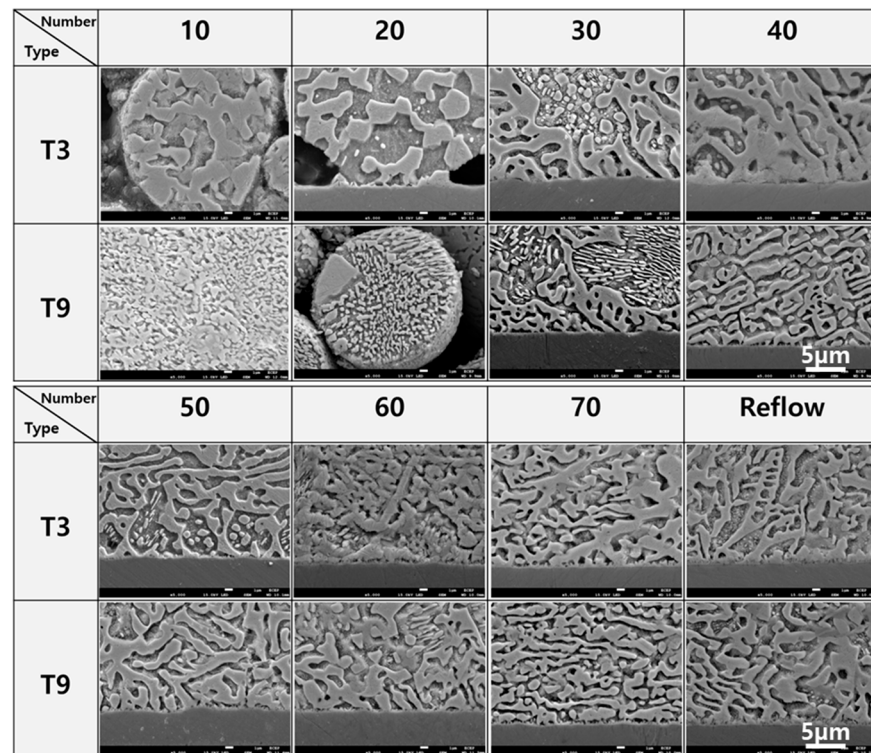


Figure 4. Changes in microstructure of Sn-58Bi solders with increasing sessions of IPL irradiation (3 Hz, 2 ms).

As IPL reached 30–40 sessions, the emergence of interparticle bonding and the coarsening of lamellar structures within the particles became increasingly apparent. Particularly in the case of T9, the microstructure following 30 IPL iterations exhibited a coexistence of regions characterized by submicron-sized lamellae and coarsened regions featuring lamellae several micrometers wide. Subsequent IPL irradiation sessions led to a predominant transformation of the microstructure, where the solder area predominantly comprised coarsened regions. Beyond 50 IPL sessions, discerning differences in microstructural features between T3 and T9 became challenging.

It is established that the reaction between Sn-58Bi solder and ENIG results in the formation of Ni_3Sn_4 IMCs at the interface [17–24]. Initially, when the number of IPL irradiation sessions is limited, the thickness of the formed IMC remains minimal. However, as the number of irradiation sessions increases to 70, Ni_3Sn_4 IMCs with thicknesses comparable to those observed in conventional reflow soldering can be discerned at the interface. Notably, the degree of IMC formation appears independent of the solder particle size, indicating a consistent reaction mechanism across different particle sizes.

3.2. Correlation between Microstructure and Mechanical Properties of Sn-58Bi Solder

The morphological features of the Sn-58Bi/ENIG reaction interfaces following 70 rounds of IPL irradiation and conventional reflow processing are depicted in Figure 5. Post 70 IPL rounds, a thin layered structure of Ni_3Sn_4 IMCs can be observed at the interface, alongside the presence of a minor quantity of feather-shaped IMCs within the Sn-rich region within the solder matrix. In contrast, after the reflow process, rod-shaped Ni_3Sn_4 IMCs are evident at the interface, accompanied by a notable abundance of feather-shaped IMCs distributed throughout the solder volume. Notably, a distinct P-rich layer atop the Ni-P layer is prominently visible in the reflow specimen, presenting as a thin, dark band [25–28]. Conversely, this P-rich layer is conspicuously absent from the IPL specimen. These observations suggest a heightened level of chemical reactivity occurring at the Sn-58Bi/ENIG interface during the conventional reflow process.

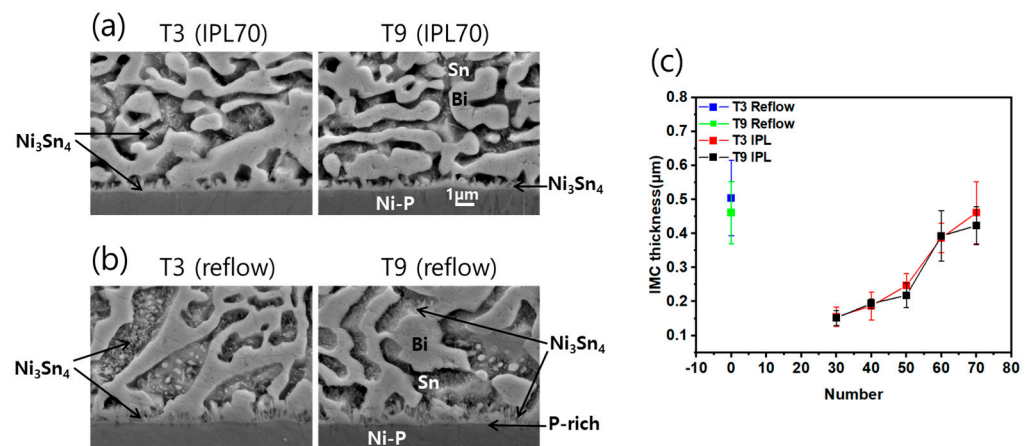


Figure 5. Close observation of the Ni_3Sn_4 IMCs formed at the Sn-58Bi/ENIG interface after 70 IPL sessions (a) and after the reflow process (b). (c) Measured thickness of the Ni_3Sn_4 IMCs.

During the IPL process, the intermittent application of instantaneous light followed by rapid cooling cycles leads to inadequate interdiffusion between the solder and ENIG. In contrast, the reflow process maintains the solder in a molten state for an extended duration, facilitating sufficient interdiffusion between the solder and ENIG. Consequently, once Ni atoms are introduced into the solder, they can diffuse over an extended period and react with Sn to form additional Ni_3Sn_4 IMCs within the solder matrix.

Initially, the thickness of Ni_3Sn_4 IMCs formed at the interface during the IPL process is minimal, and the growth rate is sluggish. However, after 50 IPL irradiation sessions, the IMC growth rate accelerates significantly compared to the initial stages of the reaction, as shown in Figure 5c. Nonetheless, even after 70 IPL irradiation sessions, the overall thickness of the IMCs remains inferior to that observed in the reflow process.

Following IPL and reflow soldering, EBSD analysis was conducted to assess the microstructural characteristics and grain orientation within the solder specimens. Phase maps and inverse pole figures (IPFs) for each solder variant were generated, as depicted in Figure 6. In the phase map, the red region signifies Sn while the green region corresponds to Bi. Post-IPL and reflow soldering, discernible variations in grain orientation were observed within the solder specimens.

Upon IPL soldering for 40 cycles, the orientation of Sn grains was situated within the intermediary region between the (001) and (110) planes in both T3 and T9 specimens. With an increase in the number of IPL irradiation sessions to 70, T9 specimens maintained a similar orientation, while T3 specimens exhibited an orientation spanning from (001) to (100). Conversely, after reflow soldering, a dominance of orientation within the intermediate region of the (100) and (110) planes was observed in both T3 and T9 specimens, with the left-hand side of T9 grains exhibiting a direct (110) orientation in addition.

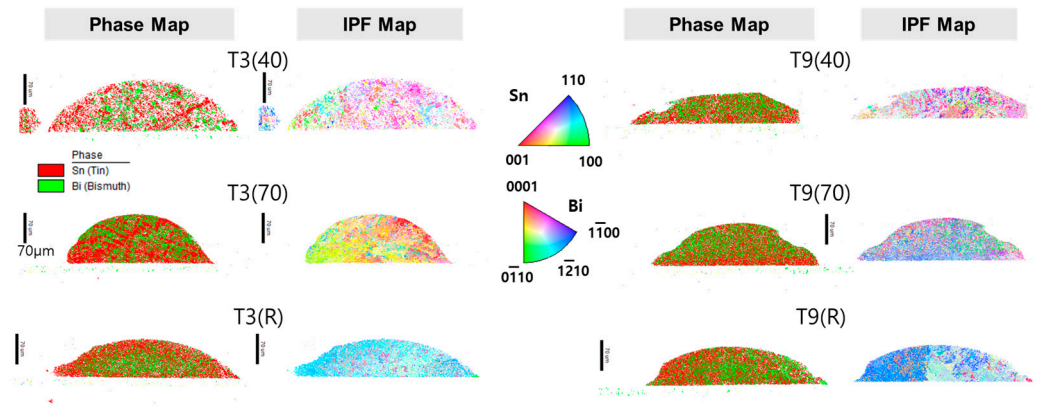


Figure 6. Results of EBSD analysis for the specimens fabricated with IPL soldering (after 40 and 70 sessions) and reflow soldering.

Regarding Bi grains, the $(1\bar{2}10)$ orientation emerged as the predominant orientation across all specimens, irrespective of the soldering method employed. Additionally, the presence of the (0001) orientation was noted alongside the $(1\bar{2}10)$ orientation exclusively within the grains of 70-IPL-session specimens. This observed shift in solder grain orientation contingent upon the soldering method or degree of irradiation presents an intriguing discovery warranting further investigation.

Figure 7 illustrates the variations in average Sn grain size and hardness across each solder variant, as determined through EBSD analysis and hardness testing. The average grain size was quantified based on the enumeration and dimensions of grains within a $180 \times 550 \mu\text{m}^2$ area of each specimen. Notably, the grain size of Sn, constituting the solder, exhibited a nadir at 40 IPL sessions, subsequently increasing with additional IPL irradiation sessions. Conversely, the hardness value displayed a maximum at 40 IPL sessions, declining with escalating IPL irradiation counts.

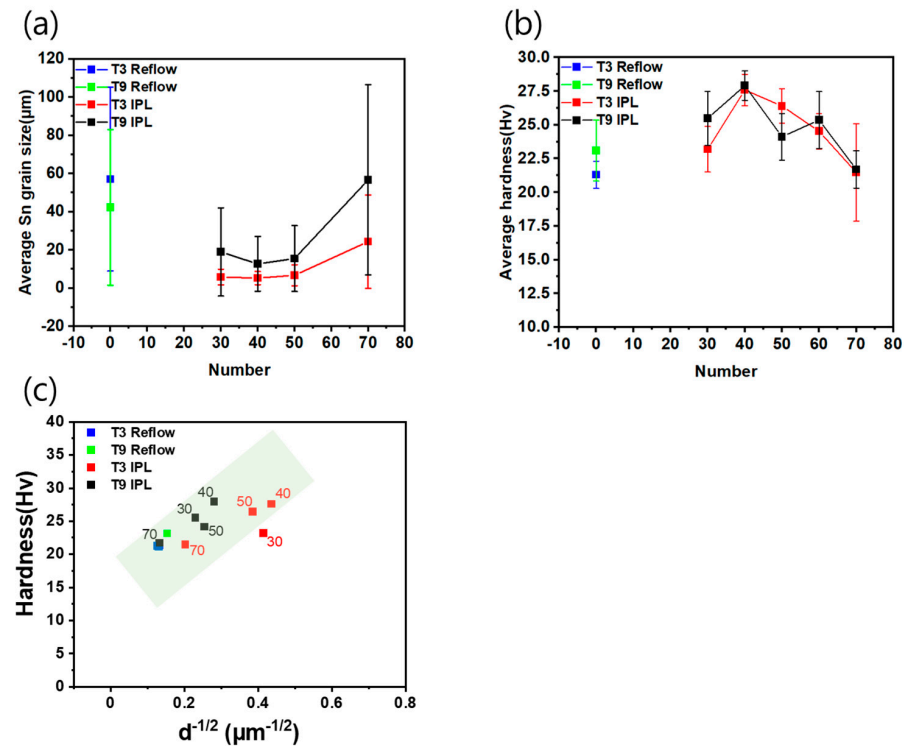


Figure 7. (a) Average Sn grain size and (b) average hardness measured for the solders fabricated by IPL or reflow soldering; (c) Hall–Petch relationship taken from the measured grain size and hardness.

It is widely acknowledged that as the microstructure coarsens, mechanical properties such as hardness and strength tend to degrade [29–33]. Specifically, hardness often conforms to the well-established Hall–Petch relationship, which correlates hardness with the inverse square root of grain size [29,30].

$$H = H_0 + kd^{-1/2} \quad (1)$$

where H is hardness and d the average grain size. H_0 and k are constants. Figure 7c displays a graph illustrating the relationship between the inverse square root of average grain size ($d^{-1/2}$) and hardness (H), as determined by substituting the measured grain size and hardness values from each solder variant produced via IPL and reflow soldering into the Hall–Petch relationship. Overall, it is evident that, with the exception of the IPL T3 specimen irradiated 30 times, the graph demonstrates a predominantly linear correlation between $d^{-1/2}$ and H , thus adhering to the Hall–Petch relationship.

In the realm of solder compositions, studies have highlighted that mechanical strength tends to improve with the refinement of the internal structure. For instance, Li et al. [32] investigated composite solders comprising Sn-58%Bi alloyed with 0, 0.03, 0.05, and 0.1 wt% Cu_6Sn_5 nanoparticles. They observed that the addition of Cu_6Sn_5 nanoparticles, particularly those sized at 10 nm, led to microstructural refinement of the Sn-58%Bi solder, with the solder containing 0.05 wt% Cu_6Sn_5 nanoparticles exhibiting superior performance. This enhancement in solder strength was attributed to the refinement of matrix phases, aligning with the principles outlined in the Hall–Petch equation. Similarly, Zhang et al. [33] demonstrated that Ga additions in Sn-XGa alloys (where X = 0.5, 1.0, 2.0 wt%) could moderately refine β -Sn grains while rendering the alloys more prone to recrystallization during cross-sectioning and polishing processes. Notably, Sn-1.0Ga exhibited significantly elevated yields and tensile strengths compared to pure Sn, attributed to the robust solid-solution strengthening effect of Ga and the refinement of β -Sn grains.

In this study, an intriguing observation was made where, despite an increase in the number of IPL irradiation sessions from 30 to 40 during the initial stages of the IPL process, the hardness of Sn-58Bi solders exhibited an increase, contrary to the expectations based on the Hall–Petch relationship. This anomaly is believed to be associated with the densification of the solders. As depicted in Figure 3, the solder initially possessed a coarse microstructure with internal voids at 30 IPL sessions, gradually transitioning into a denser structure with diminishing voids as the number of IPL sessions increased. This transformation in the microstructure of the solder likely contributed to the enhancement of its mechanical properties.

Min et al. [13] explored the feasibility of IPL soldering for BGA package assembly under varying IPL soldering conditions. During the soldering process, Ag and Cu components within the Sn-3.0Ag-0.5Cu solder underwent transformation into Ag_3Sn and Cu_6Sn_5 IMCs. At lower IPL energies (or fewer irradiation sessions), partially unreacted Ag was detected within the solders, resulting in lower shear strength and hardness values. However, with an increase in IPL energy (or irradiation count), complete transformation of Ag to Ag_3Sn occurred, leading to improved strength and hardness. From these findings, it can be inferred that during the initial stages of the IPL soldering process, all solder particles melt and coalesce into a unified lump, yet the resulting solder lump may still exhibit an immature microstructure. The specimens subjected to 30 IPL sessions in this study likely resembled such cases, displaying an immature structure characterized by internal voids and consequently exhibiting lower hardness values. The deviation of the 30-IPL specimen from the linear relationship depicted in Figure 7c can thus be attributed to this phenomenon.

4. Conclusions

In this study, Sn-58Bi solder with two different particle sizes of 1–8 μm (T9) and 25–45 μm (T3) was used and the number of IPL irradiation sessions was increased under the frequency and pulse width conditions of 3 Hz and 2.0 ms. Through an examination of alterations in solder microstructure and hardness, the following conclusions were drawn.

- (1) As the number of IPL irradiation sessions increases, the initial solder particles gradually agglomerate and aggregate into a single lump after 30 irradiation sessions. After 30–40 IPL sessions, a large number of voids was observed overall inside the T3 solder, and a small number of round voids was discovered at the interface with ENIG in T9.
- (2) After IPL soldering, a thin layered structure of Ni₃Sn₄ IMC forms at the Sn-58Bi/ENIG interface, and the P-rich layer is not prominently visible. In contrast, after reflow soldering, rod-shaped Ni₃Sn₄ IMCs are abundantly formed not only at the reaction interface but also within the solder bulk, accompanied by the notable presence of a P-rich layer beneath the IMC.
- (3) After IPL soldering, the orientation of Sn grains is situated within the intermediary region between the (001) and (110) planes. On the other hand, after reflow soldering, a dominance of orientation within the intermediate region of the (100) and (110) planes can be observed. Regarding Bi grains, the (1 $\bar{2}$ 10) orientation emerges as the predominant orientation across all specimens, irrespective of the soldering method employed.
- (4) During IPL soldering, as the number of irradiation sessions increases gradually, a progression from an immature to a fine to a coarsened microstructure occurs in the solder. Consequently, the mechanical strength (hardness) of the solder exhibits a tendency to initially increase slightly, before decreasing. The hardness measured in the immature stage may deviate slightly from the range predicted by the Hall–Petch relationship.
- (5) Based on the experimental findings, for IPL at a frequency of 3 Hz and a pulse width of 2 ms, optimal outcomes were achieved within the IPL exposure range of 40–50 sessions, characterized by a diminutive grain size, elevated hardness, and minimal IMC thickness.

Author Contributions: Conceptualization, methodology, writing—original draft, and funding acquisition, Y.S.; investigation, methodology, and funding acquisition, H.G.; investigation, data curation, and visualization, T.N.; methodology, writing—review editing, and formal analysis, S.-B.J. and Y.S. All authors have read and agreed to the published version of the manuscript.

Funding: This study was supported by a research fund from Chosun University, 2022.

Data Availability Statement: The original contributions presented in the study are included in the article, further inquiries can be directed to the corresponding author/s.

Conflicts of Interest: The authors declare no conflicts of interest.

References

1. Feldmann, K.; Franke, J.; Schüßler, F. Development of micro assembly processes for further miniaturization in electronics production. *CIRP Ann.* **2010**, *59*, 1–4. [[CrossRef](#)]
2. Sitaraman, S.; Sukumaran, V.; Pulugurtha, M.R.; Wu, Z.; Suzuki, Y.; Kim, Y.; Sundaram, V.; Kim, J.; Tummala, R.R. Miniaturized bandpass filters as ultrathin 3-D IPDs and embedded thinfilms in 3-D glass modules. *IEEE Trans. Compon. Packag. Manuf. Technol.* **2017**, *7*, 1410–1418. [[CrossRef](#)]
3. Kim, M.S.; Pulugurtha, M.R.; Kim, Y.; Park, G.; Cho, K.; Smet, V.; Sundaram, V.; Kim, J.; Tummala, R. Miniaturized and high-performance RF packages with ultra-thin glass substrates. *Microelectron. J.* **2018**, *77*, 66–72. [[CrossRef](#)]
4. Zhang, P.; Xue, S.; Wang, J. New challenges of miniaturization of electronic devices: Electromigration and thermomigration in lead-free solder joints. *Mater. Des.* **2020**, *192*, 108726. [[CrossRef](#)]
5. Xiong, M.Y.; Zhang, L. Interface reaction and intermetallic compound growth behavior of Sn-Ag-Cu lead-free solder joints on different substrates in electronic packaging. *J. Mater. Sci.* **2019**, *54*, 1741–1768. [[CrossRef](#)]
6. Lau, C.S.; Khor, C.Y.; Soares, D.; Teixeira, J.C.; Abdullah, M.Z. Thermo-mechanical challenges of reflowed lead-free solder joints in surface mount components: A review. *Solder. Surf. Mt. Technol.* **2016**, *39*, 88. [[CrossRef](#)]
7. Feng, J.; Xu, D.E.; Tian, Y.; Mayer, M. SAC305 solder reflow: Identification of melting and solidification using in-process resistance monitoring. *IEEE Trans. Compon. Packag. Manuf. Technol.* **2019**, *9*, 1623–1631. [[CrossRef](#)]
8. Jung, Y.; Ryu, D.; Gim, M.; Kim, C.; Song, Y.; Kim, J.; Yoon, J.; Lee, C. Development of Next Generation Flip Chip Interconnection Technology Using Homogenized Laser-Assisted Bonding. In Proceedings of the IEEE 66th Electronic Components and Technology Conference (ECTC), Las Vegas, NV, USA, 31 May–3 June 2016; pp. 88–94.
9. Tian, W.; Ma, Z.; Cao, X.; Lin, J.; Cui, Y.; Huang, X. Application of metal interconnection process with micro-LED display by laser-assisted bonding technology. *J. Mater. Sci. Mater. Electron.* **2023**, *34*, 2253. [[CrossRef](#)]

10. Kim, S.; Yu, D.; Kim, Y.; Son, J.; Byun, D.; Bang, J. Interfacial Properties of Sn-Cu-xCr Alloy using Laser-Assisted Bonding. *J. Weld. Join.* **2023**, *41*, 291–298. [[CrossRef](#)]
11. Jung, K.H.; Min, K.D.; Lee, C.J.; Jeong, H.; Kim, J.H.; Jung, S.B. Ultrafast Photonic Soldering with Sn–58Bi Using Intense Pulsed Light Energy. *Adv. Eng. Mater.* **2020**, *22*, 2000179. [[CrossRef](#)]
12. Ha, E.; Min, K.D.; Lee, S.; Hwang, J.S.; Kang, T.; Jung, S.B. Intense Pulsed Light Soldering of Sn–3.0Ag–0.5Cu Ball Grid Array Component on Au/Pd(P)/Ni(P) Surface-Finished Printed Circuit Board and Its Drop Impact Reliability. *Adv. Eng. Mater.* **2023**, *25*, 10. [[CrossRef](#)]
13. Min, K.D.; Ha, E.; Lee, S.; Hwang, J.S.; Kang, T.; Joo, J.; Jung, S.B. Proposal of intense pulsed light soldering process for improving the drop impact reliability of Sn–3.0Ag–0.5Cu ball grid array package. *J. Manuf. Process.* **2023**, *98*, 19–28. [[CrossRef](#)]
14. Jang, J.H.; Lee, C.J.; Hwang, B.U.; Min, K.D.; Kim, J.H.; Jung, S.B. Microstructural evolution and mechanical properties of SAC305 with the intense pulsed light soldering process under high-temperature storage test. In Proceedings of the IEEE 71st Electronic Components and Technology Conference (ECTC), Virtual, 1 June–4 July 2021; pp. 2314–2319.
15. Ho, M.J.; Li, Y.; Liu, L.; Li, Y.; Gao, C. Study of an Ultra-fast Photonic Soldering Technology without Thermal Damage in Display Module Package. *SID Symp. Dig. Tech. Pap.* **2021**, *52*, 115–118. [[CrossRef](#)]
16. Jang, Y.R.; Jeong, R.; Kim, H.S.; Park, S.S. Fabrication of solderable intense pulsed light sintered hybrid copper for flexible conductive electrodes. *Sci. Rep.* **2021**, *11*, 14551. [[CrossRef](#)] [[PubMed](#)]
17. Myung, W.R.; Kim, Y.; Jung, S.B. Evaluation of the bondability of the epoxy-enhanced Sn-58Bi solder with ENIG and ENEPIG surface finishes. *J. Electron. Mater.* **2015**, *44*, 4637–4645. [[CrossRef](#)]
18. Choi, H.; Kim, C.L.; Sohn, Y. Diffusion Barrier Properties of the Intermetallic Compound Layers Formed in the Pt Nanoparticles Alloyed Sn-58Bi Solder Joints Reacted with ENIG and ENEPIG Surface Finishes. *Materials* **2022**, *15*, 8419. [[CrossRef](#)] [[PubMed](#)]
19. Lee, S.M.; Yoon, J.W.; Jung, S.B. Electromigration effect on Sn-58% Bi solder joints with various substrate metallizations under current stress. *J. Mater. Sci. Mater. Electron.* **2016**, *27*, 1105–1112. [[CrossRef](#)]
20. Chen, C.; Wang, C.; Sun, H.; Yin, H.; Gao, X.; Xue, H.; Ni, D.; Bian, K.; Gu, Q. Interfacial Microstructure and Mechanical Reliability of Sn-58Bi/ENEPIG Solder Joints. *Processes* **2022**, *10*, 295. [[CrossRef](#)]
21. Kim, J.; Park, D.Y.; Ahn, B.; Bang, J.; Kim, M.S.; Park, H.S.; Sohn, Y.; Ko, Y.H. Effective (Pd, Ni)Sn₄ diffusion barrier to suppress brittle fracture at Sn-58Bi-xAg solder joint with Ni(P)/Pd(P)/Au metallization pad. *Microelectron. Reliab.* **2022**, *129*, 114472. [[CrossRef](#)]
22. Hao, Q.; Tan, X.F.; McDonald, S.D.; Sweatman, K.; Akaiwa, T.; Nogita, K. Investigating the Effects of Rapid Precipitation of Bi in Sn on the Shear Strength of BGA Sn-Bi Alloys. *J. Electron. Mater.* **2024**, *53*, 1223–1238. [[CrossRef](#)]
23. Zhou, S.; He, S.; Nishikawa, H. Effect of Zn addition on interfacial reactions and mechanical properties between eutectic Sn58Bi solder and ENIG substrate. *J. Nanosci. Nanotechnol.* **2020**, *20*, 106–112. [[CrossRef](#)] [[PubMed](#)]
24. Fan, Y.; Wu, Y.; Dale, T.F.; Lakshminarayana, S.A.P.; Greene, C.V.; Badwe, N.U.; Aspandiar, R.F.; Blendell, J.E.; Subbarayan, G.; Handwerker, C.A. Influence of Pad Surface Finish on the Microstructure Evolution and Intermetallic Compound Growth in Homogeneous Sn-Bi and Sn-Bi-Ag Solder Interconnects. *J. Electron. Mater.* **2021**, *50*, 6615–6628. [[CrossRef](#)]
25. Elsener, B.; Crobu, M.; Scorciapino, M.A.; Rossi, A. Electroless deposited Ni–P alloys: Corrosion resistance mechanism. *J. Appl. Electrochem.* **2008**, *38*, 1053–1060. [[CrossRef](#)]
26. Liu, P.L.; Xu, Z.; Shang, J.K. Thermal stability of electroless-nickel/solder interface: Part A. Interfacial chemistry and microstructure. *Metall. Mater. Trans. A* **2000**, *31*, 2857–2866. [[CrossRef](#)]
27. Lin, J.D.; Chou, C.T. The influence of phosphorus content on the microstructure and specific capacitance of etched electroless Ni-P coatings. *Surf. Coat. Technol.* **2019**, *368*, 126–137. [[CrossRef](#)]
28. Alam, M.O.; Chan, Y.C.; Hung, K.C. Reliability study of the electroless Ni–P layer against solder alloy. *Microelectron. Reliab.* **2002**, *42*, 1065–1073. [[CrossRef](#)]
29. Fecht, H.J.; Hellstern, E.; Fu, Z.; Johnson, W.L. Nanocrystalline metals prepared by high-energy ball milling. *Metall. Trans. A* **1990**, *21*, 2333. [[CrossRef](#)]
30. Zheng, Z.; Chiang, P.C.; Huang, Y.T.; Wang, W.T.; Li, P.C.; Tsai, Y.H.; Chen, C.M.; Feng, S.P. Study of grain size effect of Cu metallization on interfacial microstructures of solder joints. *Microelectron. Reliab.* **2019**, *99*, 44–51. [[CrossRef](#)]
31. Kang, H.; Rajendran, S.H.; Jung, J.P. Low Melting Temperature Sn-Bi Solder: Effect of Alloying and Nanoparticle Addition on the Microstructural, Thermal, Interfacial Bonding, and Mechanical Characteristics. *Metals* **2021**, *11*, 364. [[CrossRef](#)]
32. Li, J.F.; Agyakwa, P.A.; Johnson, C.M. A numerical method to determine interdiffusion coefficients of Cu₆Sn₅ and Cu₃Sn intermetallic compounds. *Intermetallics* **2013**, *40*, 50–59. [[CrossRef](#)]
33. Zhang, H.; Ma, Z.; Yang, S.; Fan, M.; Cheng, X. Microstructure and mechanical properties of Sn-xGa alloys and solder joints. *J. Mater. Res. Technol.* **2023**, *26*, 3830–3839. [[CrossRef](#)]

Disclaimer/Publisher’s Note: The statements, opinions and data contained in all publications are solely those of the individual author(s) and contributor(s) and not of MDPI and/or the editor(s). MDPI and/or the editor(s) disclaim responsibility for any injury to people or property resulting from any ideas, methods, instructions or products referred to in the content.